

# Quantum circuit-like learning: A fast and scalable classical machine-learning algorithm with similar performance to quantum circuit learning

Naoko Koide-Majima<sup>a†</sup>, Kei Majima<sup>b†</sup>

<sup>a</sup>National Institute of Information and Communications Technology, Osaka 565-0871, Japan

<sup>b</sup>Graduate School of Informatics, Kyoto University, Kyoto 606-8501, Japan

† These authors contributed equally to this work.

The application of near-term quantum devices to machine learning (ML) has attracted much attention. In one such attempt, Mitarai et al. (2018) proposed a framework to use a quantum circuit for supervised ML tasks, which is called quantum circuit learning (QCL). Due to the use of a quantum circuit, QCL can employ an exponentially high-dimensional Hilbert space as its feature space. However, its efficiency compared to classical algorithms remains unexplored. In this study, using a statistical technique called “count sketch,” we propose a classical ML algorithm that uses the same Hilbert space. In numerical simulations, our proposed algorithm demonstrates similar performance to QCL for several ML tasks. This provides a new perspective with which to consider the computational and memory efficiency of quantum ML algorithms.

## I. INTRODUCTION

Because quantum computers with tens or hundreds of qubits are becoming available, their application to machine learning has attracted much attention. Such quantum devices are called noisy intermediate-scale quantum (NISQ) devices [1], and many quantum-classical hybrid algorithms have been proposed to use NISQ devices efficiently. For example, the variational quantum eigensolver (VQE) has recently been used to find the ground state of a given Hamiltonian [2–5] and the quantum approximate optimization algorithm (QAOA) enables us to obtain approximate solutions to combinatorial optimization problems [6–8]. More recently, several studies have proposed algorithms that use NISQ devices for machine-learning tasks [9–29], some of which have been experimentally tested using actual quantum devices [30–36].

In one such attempt, Mitarai et al. [26] proposed a framework to train a parameterized quantum circuit for supervised classification and regression tasks; this is called quantum circuit learning (QCL). In QCL, input data (*i.e.*, feature vectors) are nonlinearly mapped into a  $2^Q$ -dimensional Hilbert space, where  $Q$  is the number of qubits, and then a parameterized unitary transformation is applied to the mapped data (see Section II for details). The parameters of the unitary transformation are tuned to minimize a given cost function (*i.e.*, a prediction error). QCL employs the high-dimensional Hilbert spaces implemented by quantum circuits; however, its computational and memory efficiency compared to classical algorithms remains uncertain.

In this study, we present a machine-learning algorithm with similar properties to QCL whose computational time and required memory size are linear with respect to the hyperparameter corresponding to the number of qubits, which we refer to as quantum circuit-like learning (QCLL). To implement this algorithm, we use a statistical technique

known as “count sketch” [37–40]. Given a high-dimensional vector space, the count sketch technique provides a projection from the given space to a lower dimensional space that approximately preserves the inner product in the original space (see Section II for details). Therefore, this enables us to use the same  $2^Q$ -dimensional Hilbert space as the feature space with a low computational cost. To demonstrate the similarities between QCL and QCLL as machine-learning algorithms, we perform numerical simulations in which these two algorithms are applied to several machine-learning tasks. Our numerical results demonstrate that the behavior and performance of QCLL are very similar to those of QCL. We believe that our proposed algorithm and simulation results provide a new perspective with which to consider the computational and memory efficiency of quantum machine learning algorithms.

## II. ALGORITHM

This section is organized as follows. First, we introduce QCL based on the work of Mitarai et al. [26]. In the following subsection, we explain the count sketch technique, which is used in QCLL. Finally, we explain QCLL. Note that a Python implementation of QCLL is available at our GitHub repository [<https://github.com/nkmjm/>].

### A. Quantum circuit learning

Here, we introduce the QCL framework proposed by Mitarai et al. [26]. In supervised learning, an algorithm is given a training dataset  $\mathcal{D} = \{(\mathbf{x}_n, y_n)\}_{n=1}^N$  of  $N$  pairs of  $D$ -dimensional real input vectors  $\mathbf{x}_n \in \mathbb{R}^D$  and target outputs  $y_n$ . The outputs  $y_n$  take continuous values in the case of regression and discrete values in the case of classification. The algorithm is required to predict the target output for a new input vector  $\mathbf{x}_{\text{new}} \in \mathbb{R}^D$ . In QCL, the prediction model is constructed using a quantum circuit with

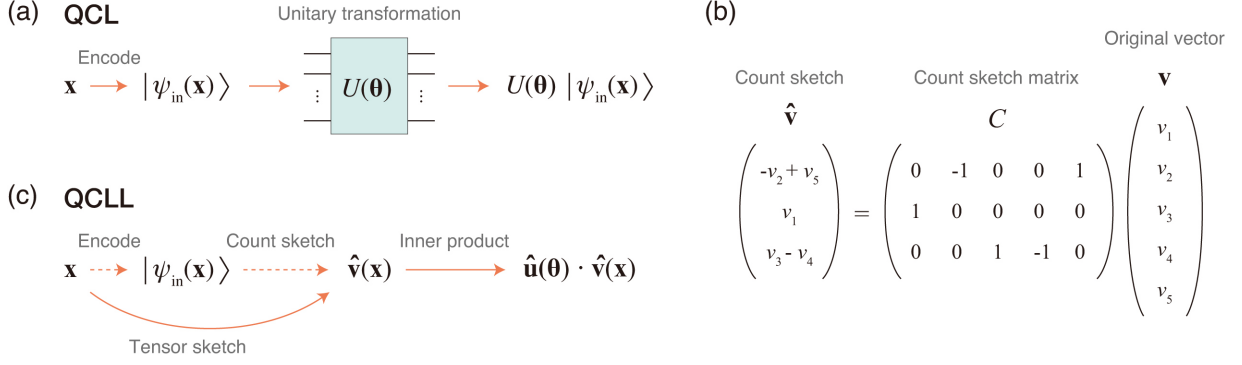


**FIG. 1.** Quantum circuit learning (QCL) and quantum circuit-like learning (QCLL). (a) Flowchart of QCL. In QCL, an input vector is encoded (mapped) into a quantum state and then a parameterized unitary transformation is applied to it. (b) Count sketch technique. An example of a  $3 \times 5$  count sketch matrix is shown. This provides a projection from a five-dimensional space to a three-dimensional space. (c) Flowchart of QCLL. In QCLL, the count sketch of the quantum state vector that encodes an input vector is computed by the tensor sketch algorithm. The tensor sketch algorithm enables us to perform this computation without accessing the quantum state vector, which is typically high dimensional. Then, the inner product between the resultant count sketch and a parameterized unit vector is computed as the output.

multiple learnable parameters as follows (see also Figure 1(a))

1. Encode input vectors  $\mathbf{x}_n$  ( $n = 1, \dots, N$ ) into quantum states  $|\psi_{\text{in}}(\mathbf{x}_n)\rangle = U_{\text{enc}}(\mathbf{x}_n)|0\rangle^{\otimes Q}$  by applying unitary gates  $U_{\text{enc}}(\mathbf{x}_n)$  to the initialized state  $|0\rangle^{\otimes Q}$ .
2. Apply a  $\theta$ -parameterized unitary  $U(\theta)$  to the states  $|\psi_{\text{in}}(\mathbf{x}_n)\rangle$  and generate the output states  $|\psi_{\text{out}}(\mathbf{x}_n, \theta)\rangle = U(\theta)|\psi_{\text{in}}(\mathbf{x}_n)\rangle$ .
3. Measure the expectation values of a predefined observable  $B$  for the output states  $|\psi_{\text{out}}(\mathbf{x}_n, \theta)\rangle$ . Using a predefined function  $F(\cdot)$ , a scaling parameter  $a$ , and an intercept parameter  $b$ , the predictions from this machine-learning model are defined as

$$\hat{y}_n = F(a\langle\psi_{\text{out}}(\mathbf{x}_n, \theta)|B|\psi_{\text{out}}(\mathbf{x}_n, \theta)\rangle + b). \quad (1)$$

4. Minimize the cost function

$$C(a, b, \theta) = \sum_{n=1}^N E(y_n, \hat{y}_n) \quad (2)$$

with respect to the parameters  $(a, b, \theta)$ , where  $E(\cdot, \cdot): \mathbb{R} \times \mathbb{R} \rightarrow \mathbb{R}$  is a function to measure the prediction error.

5. Make a prediction for a new input vector  $\mathbf{x}_{\text{new}}$  by computing

$$F(a\langle\psi_{\text{out}}(\mathbf{x}_{\text{new}}, \theta)|B|\psi_{\text{out}}(\mathbf{x}_{\text{new}}, \theta)\rangle + b). \quad (3)$$

In step 1 above, the input vectors are nonlinearly mapped into a  $2^Q$ -dimensional Hilbert space, where  $Q$  is the number of qubits used for encoding. In Mitarai et al. [26],

the unitary gates  $U_{\text{enc}}(\mathbf{x}_n)$  were constructed using rotations of individual qubits around the y-axis. Following their procedure, in this study, we treat a case in which a given input vector  $\mathbf{x} = (x_1, \dots, x_D)^T \in \mathbb{R}^D$  is encoded in

$$|\psi_{\text{in}}(\mathbf{x})\rangle = \otimes_{d=1}^D \left\{ \otimes_{q_d=1}^{Q_d} \left( x_d, \sqrt{1 - x_d^2} \right)^T \right\}, \quad (4)$$

where  $Q_d$  is the number of qubits used to encode the  $d$ -th element of the vector  $\mathbf{x}$ . Note that  $Q = \sum_{d=1}^D Q_d$ . The elements of the vector  $|\psi_{\text{in}}(\mathbf{x})\rangle$  include high-order polynomials such as  $x_d^{Q_d}$ ; this introduces nonlinearity into the prediction model.

In step 2, a parameterized unitary transformation  $U(\theta)$  is applied to the states prepared in step 1. In Mitarai et al. [26], this unitary transformation was constructed as a chain of rotations of individual qubits and random unitary transformations. Following their procedure here, we assume a case where  $U(\theta)$  takes the form

$$U(\theta) = R_M(\theta)U_M R_{M-1}(\theta)U_{M-1} \cdots R_1(\theta)U_1, \quad (5)$$

where  $M$  is the depth of the quantum circuit,  $R_1(\theta), \dots, R_M(\theta)$  are rotations of individual qubits whose angles are specified by elements of  $\theta$ , and  $U_1, \dots, U_M$  are random unitary transformations. As a result, each element of the output vector (*i.e.*, the output state)  $|\psi_{\text{out}}(\mathbf{x}, \theta)\rangle$  has the form of the inner product between  $|\psi_{\text{in}}(\mathbf{x})\rangle$  and a unit vector randomly parameterized by  $\theta$ . In other words, when we denote  $|\psi_{\text{in}}(\mathbf{x})\rangle$  and  $|\psi_{\text{out}}(\mathbf{x}, \theta)\rangle$  by

$$\mathbf{v}_{\text{in}}(\mathbf{x}) = \left( v_{\text{in},1}(\mathbf{x}), \dots, v_{\text{in},2^Q}(\mathbf{x}) \right)^T$$

and

$$\mathbf{v}_{\text{out}}(\mathbf{x}, \boldsymbol{\theta}) = \left( v_{\text{out},1}(\mathbf{x}, \boldsymbol{\theta}), \dots, v_{\text{out},2^Q}(\mathbf{x}, \boldsymbol{\theta}) \right)^T,$$

each element of  $|\psi_{\text{out}}(\mathbf{x}, \boldsymbol{\theta})\rangle$  has the form

$$v_{\text{out},i}(\mathbf{x}, \boldsymbol{\theta}) = \mathbf{u}_i(\boldsymbol{\theta}) \cdot \mathbf{v}_{\text{in}}(\mathbf{x}) \quad (i = 1, \dots, 2^Q), \quad (6)$$

where  $\mathbf{u}_i(\boldsymbol{\theta})$  is a unit vector randomly parameterized by  $\boldsymbol{\theta}$ .

The predefined function  $F(\cdot)$  and the loss function  $E(\cdot, \cdot)$  used in steps 3 and 4 are manually defined. In a regression task,  $F(x) = x$  and  $E(y, \hat{y}) = (y - \hat{y})^2$  are often used. In a classification task, the softmax and cross-entropy functions are often used. To minimize the cost function  $C(a, b, \boldsymbol{\theta})$ , gradient-based methods [26] or gradient-free optimization methods, such as Nelder–Mead [2], are used. Optionally, a recently proposed, more efficient method can be used under some conditions [41].

## B. Count sketch technique

To approximately compute the inner product in the  $2^Q$ -dimensional Hilbert space in an efficient manner on classical computers, we use a technique called ‘‘count sketch.’’ In this section, we first present a theorem that shows the approximation accuracy of the count sketch technique. Then, we explain an algorithm to perform this approximation efficiently in the case where input vectors are represented as the Kronecker products of low-dimensional vectors such as those shown in Eq. (4).

Here, we assume that we want to approximate the inner product of  $K$ -dimensional vectors.

### Definition 1

Given two independent hash functions  $h: \{1, \dots, K\} \rightarrow \{1, \dots, K'\}$  and  $s: \{1, \dots, K\} \rightarrow \{+1, -1\}$ , the  $K' \times K$  matrix whose  $(k', k)$ -entry is

$$\begin{cases} s(k) & (h(k) = k') \\ 0 & (\text{otherwise}) \end{cases} \quad (7)$$

is called a count sketch matrix.

Note that, because  $h$  and  $s$  are hash functions with randomness, the count sketch matrix specified by  $h$  and  $s$  is a random matrix. According to convention, a sample (*i.e.*, an observation) drawn from a count sketch matrix is also called a count sketch matrix in this study; however, the interpretation is clear from the context. An example of a count sketch matrix is shown in Figure 1(b).

### Definition 2

Given a  $K' \times K$  count sketch matrix  $C$ , the count sketch of a  $K$ -dimensional column vector  $\mathbf{v}$  is defined as the  $K'$ -dimensional vector  $C\mathbf{v}$ .

Count sketches are random vectors. According to convention, the random vector  $C\mathbf{v}$  and a sample (*i.e.*, an observation) from  $C\mathbf{v}$  are both called the count sketch of  $\mathbf{v}$ .

Count sketch matrices have the property shown in Theorem 3; this allows us to use count sketches as compact representations of high-dimensional vectors.

### Theorem 3

We assume that  $C$  is a  $K' \times K$  count sketch matrix. Given two  $K$ -dimensional column vectors  $\mathbf{v}_1$  and  $\mathbf{v}_2$ ,

$$\mathbb{E}_C[C\mathbf{v}_1 \cdot C\mathbf{v}_2] = \mathbf{v}_1 \cdot \mathbf{v}_2, \quad (8)$$

$$\text{Var}_C[C\mathbf{v}_1 \cdot C\mathbf{v}_2] \leq \frac{1}{K'} \{(\mathbf{v}_1 \cdot \mathbf{v}_2)^2 + \|\mathbf{v}_1\|^2 \|\mathbf{v}_2\|^2\}, \quad (9)$$

where  $\mathbb{E}_x[f(x)]$  and  $\text{Var}_x[f(x)]$  denote the expectation and variance, respectively, of a function  $f(x)$  with respect to a random variable  $x$ .

Proof: See [37,39].

Using the above property, once we obtain the count sketches of vectors, we can compute approximations of the values of the inner products of these vectors in  $O(K')$  computational time. This computational time is independent of the original dimensionality  $K$  of the space. Note that, because vectors we primarily treat in later sections are unit vectors, the variance (*i.e.*, the approximation error) is always smaller than  $2/K'$  in such a case. Based on the numerical results in a previous study [37],  $K'$  was set to 100 in the numerical experiments in this study.

Next, we describe an algorithm to compute the count sketch of a given vector efficiently when the given vector is represented as the tensor product of low-dimensional vectors. We consider a case in which we compute the count sketch of  $\mathbf{v} = \bigotimes_{q=1}^Q \mathbf{v}_q$ .

### Theorem 4

We assume that a  $D_{\text{prod}}$ -dimensional vector  $\mathbf{v}$  can be represented by

$$\mathbf{v} = \bigotimes_{q=1}^Q \mathbf{v}_q, \quad (10)$$

where  $\mathbf{v}_q$  ( $q = 1, \dots, Q$ ) are  $D_q$ -dimensional vectors, and we assume that  $C$  and  $C_q$  are  $K' \times D_{\text{prod}}$  and  $K' \times D_q$  count sketch matrices, respectively. The random vector  $C\mathbf{v}$  and the convolution of the random vectors  $C_1\mathbf{v}_1, \dots, C_Q\mathbf{v}_Q$  follow the same distribution.

Proof: See [38].

Because the convolution of vectors can be computed using a fast Fourier transform (FFT),  $C\mathbf{v}$  in the above can be computed as follows.

1. Compute  $C_q\mathbf{v}_q$  ( $q = 1, \dots, Q$ ), where  $\mathbf{v}_q$  are given

$D_q$ -dimensional vectors and  $C_q$  are  $K' \times D_q$  count sketch matrices.

2. Compute  $\text{FFT}(C_q \mathbf{v}_q)$  using FFT.
3. Compute  $\text{FFT}(C_1 \mathbf{v}_1) \odot \cdots \odot \text{FFT}(C_Q \mathbf{v}_Q)$  where  $\odot$  denotes the element-wise product.
4. Compute  $\text{FFT}^{-1}(\text{FFT}(C_1 \mathbf{v}_1) \odot \cdots \odot \text{FFT}(C_Q \mathbf{v}_Q))$ . Return this as the output of the algorithm.

According to convention, we call this algorithm ‘‘tensor sketch’’ in this paper. Note that the computation of  $C_q \mathbf{v}_q$  ( $q = 1, \dots, Q$ ) in step 1 of the tensor sketch algorithm takes  $O(K'(D_1 + D_2 + \dots + D_Q))$  computational time. This is smaller than  $O(K'D_1 D_2 \cdots D_Q)$ , which is the time for direct computation, and the computational time for steps 2–4 does not depend on the dimensionality of  $\mathbf{v}_q$  (i.e.,  $D_q$ ).

### C. Quantum circuit-like learning

Using the count sketch technique and the tensor sketch algorithm, we present a machine-learning algorithm with similar properties to QCL. As in QCL, we assume that the algorithm is given a training dataset  $\mathcal{D} = \{(\mathbf{x}_n, y_n)\}_{n=1}^N$  of  $N$  pairs of  $D$ -dimensional real input vectors  $\mathbf{x}_n = (x_{n1}, \dots, x_{nD})^T \in \mathbb{R}^D$  and target outputs  $y_n$ . The hyperparameter corresponding to the number of qubits used for encoding the  $d$ -th element of the input vectors is denoted by  $Q_d$ . The QCLL algorithm is as follows (see also Figure 1(c)).

1. Draw  $Q = \sum_{d=1}^D Q_d$  samples from a  $K' \times 2$  count sketch matrix, and compute the count sketches of  $\mathbf{v}_{\text{in}}(\mathbf{x}_n) = \otimes_{d=1}^D \left\{ \otimes_{q=1}^{Q_d} (x_{nd}, \sqrt{1 - x_{nd}^2})^T \right\}$  using the tensor sketch algorithm. Denote the resultant count sketches by  $\hat{\mathbf{v}}_{\text{in}}(\mathbf{x}_n)$ .
2. Draw  $P$  samples from a  $K' \times 2$  count sketch matrix, and compute the count sketch of  $\mathbf{u}(\boldsymbol{\theta}) = \otimes_{p=1}^P (\cos \theta_p, \sin \theta_p)^T$  using the tensor sketch algorithm. Repeat this  $I$  times, and denote the resultant count sketches by  $\hat{\mathbf{u}}_i(\boldsymbol{\theta})$  ( $i = 1, \dots, I$ ). Then, compute  $\hat{v}_{\text{out},i}(\mathbf{x}_n, \boldsymbol{\theta}) = \hat{\mathbf{u}}_i(\boldsymbol{\theta}) \cdot \hat{\mathbf{v}}_{\text{in}}(\mathbf{x}_n)$ , and denote them collectively by  $\hat{\mathbf{v}}_{\text{out}}(\mathbf{x}_n, \boldsymbol{\theta}) = (\hat{v}_{\text{out},1}(\mathbf{x}_n, \boldsymbol{\theta}), \dots, \hat{v}_{\text{out},I}(\mathbf{x}_n, \boldsymbol{\theta}))$ .
3. Using a predefined Hermitian matrix  $B$ , compute  $\hat{\mathbf{v}}_{\text{out}}(\mathbf{x}_n, \boldsymbol{\theta})^\dagger B \hat{\mathbf{v}}_{\text{out}}(\mathbf{x}_n, \boldsymbol{\theta})$ . Using a predefined function  $F(\cdot)$ , a scaling parameter  $a$ , and an intercept parameter  $b$ , the predictions from this machine-learning model are defined as

$$\hat{y}_n = F(a \hat{\mathbf{v}}_{\text{out}}(\mathbf{x}_n, \boldsymbol{\theta})^\dagger B \hat{\mathbf{v}}_{\text{out}}(\mathbf{x}_n, \boldsymbol{\theta}) + b). \quad (11)$$

4. Minimize the cost function

$$C(a, b, \boldsymbol{\theta}) = \sum_{n=1}^N E(y_n, \hat{y}_n) \quad (12)$$

with respect to the parameters  $(a, b, \boldsymbol{\theta})$ , where  $E(\cdot, \cdot): \mathbb{R} \times \mathbb{R} \rightarrow \mathbb{R}$  is a function to measure the prediction error.

5. Make a prediction for a new input vector  $\mathbf{x}_{\text{new}}$  by computing

$$F(a \hat{\mathbf{v}}_{\text{out}}(\mathbf{x}_{\text{new}}, \boldsymbol{\theta})^\dagger B \hat{\mathbf{v}}_{\text{out}}(\mathbf{x}_{\text{new}}, \boldsymbol{\theta}) + b). \quad (13)$$

In step 1 of the above algorithm,  $2^Q$ -dimensional vectors  $\otimes_{d=1}^D \left\{ \otimes_{q=1}^{Q_d} (x_{nd}, \sqrt{1 - x_{nd}^2})^T \right\}$  are encoded as the  $K'$ -dimensional vectors  $\hat{\mathbf{v}}_{\text{in}}(\mathbf{x}_n)$ . According to Theorem 3, the values of the norm of  $\hat{\mathbf{v}}_{\text{in}}(\mathbf{x}_n)$  are 1.0 on average and, for an arbitrary pair of input vectors  $\mathbf{x}_{n_1}$  and  $\mathbf{x}_{n_2}$ ,  $\hat{\mathbf{v}}_{\text{in}}(\mathbf{x}_{n_1}) \cdot \hat{\mathbf{v}}_{\text{in}}(\mathbf{x}_{n_2})$  is equal to  $\mathbf{v}_{\text{in}}(\mathbf{x}_{n_1}) \cdot \mathbf{v}_{\text{in}}(\mathbf{x}_{n_2})$  on average. This indicates that the pairwise similarities between input vectors in the  $2^Q$ -dimensional Hilbert space are approximately preserved in the  $K'$ -dimensional space constructed by this step.

In step 2, each element of  $\hat{\mathbf{v}}_{\text{out}}(\mathbf{x}_n, \boldsymbol{\theta})$  takes the same form as in Eq. (6) of QCL. The  $i$ -th element of  $\hat{\mathbf{v}}_{\text{out}}(\mathbf{x}_n, \boldsymbol{\theta})$  can be written as

$$\hat{v}_{\text{out},i}(\mathbf{x}_n, \boldsymbol{\theta}) = \hat{\mathbf{u}}_i(\boldsymbol{\theta}) \cdot \hat{\mathbf{v}}_{\text{in}}(\mathbf{x}_n) \quad (i = 1, \dots, I). \quad (14)$$

According to Theorem 3, on average,  $\hat{\mathbf{u}}_i(\boldsymbol{\theta})$  is a unit vector randomly parameterized by  $\boldsymbol{\theta}$ , which has the same property as  $\mathbf{u}_i(\boldsymbol{\theta})$  in Eq. (6) of QCL.

Note that steps 3–5 of QCLL are completely the same as those of QCL if we replace  $\hat{\mathbf{v}}_{\text{out}}(\cdot, \cdot)$  with  $|\psi_{\text{out}}(\cdot, \cdot)\rangle$ . Using the tensor sketch algorithm, we can perform QCLL in  $O(Q)$  computational time.

Similar to QCL, we can use gradient-based methods to minimize the cost function in step 4 of QCLL. To combine QCL with gradient-based methods, inspired by Li et al. [42], Mitarai et al. [26] proposed a method to calculate  $\partial \hat{y}_n / \partial \theta_p$ . Similar to their approach, in QCLL, we can calculate  $\partial \hat{v}_{\text{out},i}(\mathbf{x}_n, \boldsymbol{\theta}) / \partial \theta_p$  by evaluating  $\hat{v}_{\text{out},i}(\mathbf{x}_n, \boldsymbol{\theta} + \Delta \boldsymbol{\theta})$ , where  $\Delta \boldsymbol{\theta}$  is a vector whose  $p$ -th element is  $-\pi/2$  and whose other elements are zero. By combining this and the chain rule, we can calculate the derivative of the cost function in step 4 of QCLL.

## III. RESULTS

In this section, we demonstrate that the behavior and prediction performance of QCLL are similar to those of QCL using numerical simulations. Following the numerical simulations in Mitarai et al. [26], we treat the same regression and classification tasks using QCL and QCLL.

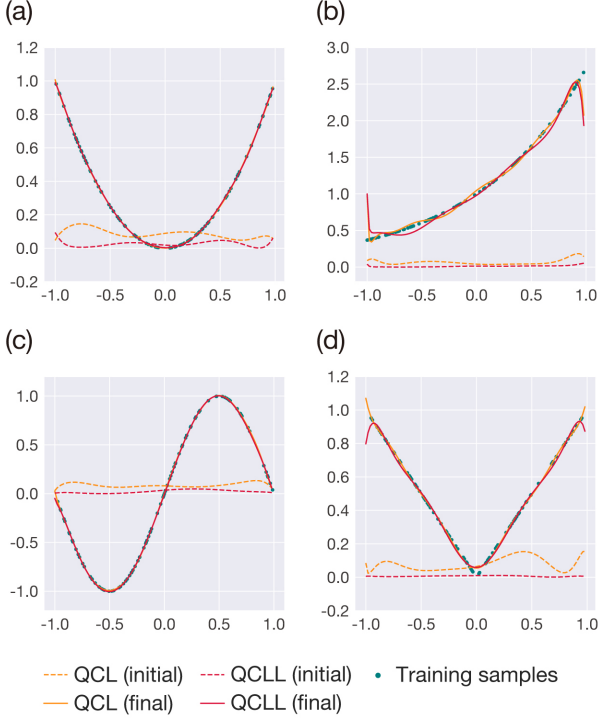


**FIG. 2.** Demonstration of the performances of QCL and QCLL on regression tasks. As regression tasks, four functions (a)  $y = x^2$ , (b)  $y = e^x$ , (c)  $y = \sin x$ , and (d)  $y = |x|$  were learned (estimated). Outputs from QCL (orange) and QCLL (red) prior to training (dashed line) and after training (solid line) are shown together with the training samples (green dots).

First, we performed a regression analysis where the functions  $f(x) = x^2$ ,  $e^x$ ,  $\sin x$ , and  $|x|$  were learned (estimated) from a given training dataset  $\mathcal{D} = \{(\mathbf{x}_n, y_n)\}_{n=1}^{100}$ . Following the procedure in Mitarai et al. [26], the input vectors  $\mathbf{x}_n$  are one-dimensional, and were randomly sampled from the range  $[-1, 1]$ . The target outputs  $y_n$  were set to  $f(\mathbf{x}_n)$ . The number of qubits ( $Q$ ) was set to six, and the depth of the quantum circuit ( $M$ ) was set to six. A matrix whose first five diagonal entries are one and whose other entries are zero was used as the predefined Hermitian matrix  $B$ . As the parameterized unitary matrix  $U(\boldsymbol{\theta})$  of QCL, we used the form of Eq. (5) with

$$R_m(\boldsymbol{\theta}) = \bigotimes_{q=1}^6 \begin{pmatrix} \cos(\theta_{6(m-1)+q}) & -\sin(\theta_{6(m-1)+q}) \\ \sin(\theta_{6(m-1)+q}) & \cos(\theta_{6(m-1)+q}) \end{pmatrix} \quad (m = 1, \dots, M)$$

and uniformly random unitary matrices  $U_m$ . The number of learnable parameters was exactly the same for QCL and QCLL. In other words,  $\boldsymbol{\theta}$  in both QCL and QCLL is a 36-dimensional vector in this numerical simulation.  $F(x) = x$  and  $E(y, \hat{y}) = (y - \hat{y})^2$  were adopted as the prede-

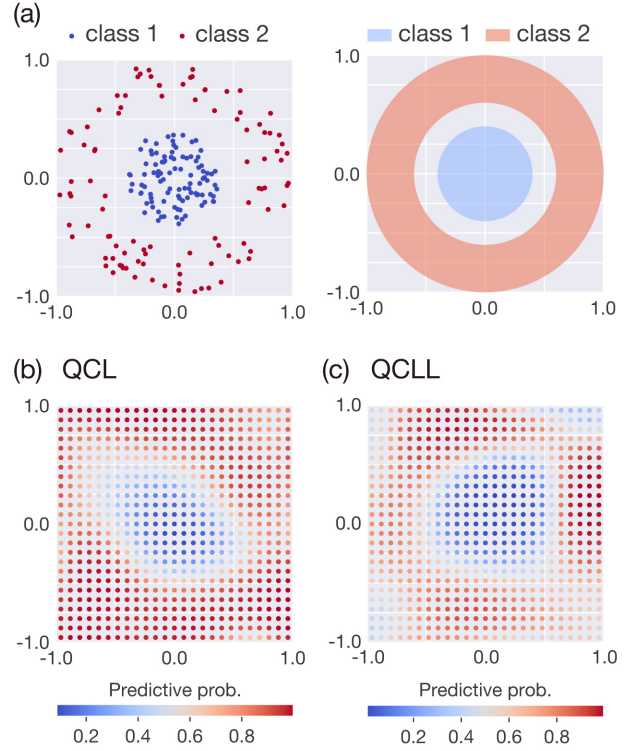


**FIG. 3.** Demonstration of the performances of QCL and QCLL on a classification task. (a) Training data in the input feature space. The blue and red dots in the left panel indicate the training samples for classes 1 and 2, respectively. These training data were uniformly sampled from the colored areas in the right panel. (b) Predictive probability from QCL after training. QCL was tuned using the training data shown in panel (a). Outputs (*i.e.*, the predictive probability) for individual grid points are shown. (c) Predictive probability from QCLL after training. The formats and procedures are the same as those in panel (b).

defined function  $F(\cdot)$  and the loss function  $E(\cdot, \cdot)$ , respectively. To minimize the cost function, we used a gradient-based method, SLSQP [43]. The number of iterations was set to 100. To avoid local minima of the cost function, for the same training data, we repeated the SLSQP algorithm 20 times with different initializations and the parameters  $(a, b, \boldsymbol{\theta})$  showing the lowest cost function value was used for the prediction. The results are shown in Figure 2. The outputs of QCL and QCLL were fitted to the target functions with similar degrees.

Next, we treated a classification task. Following the numerical simulations in Mitarai et al. [26], the simple non-linear binary classification task shown in Figure 3(a) was treated. The number of training samples was 200 (100 for class 1 and 100 for class 2). To treat this binary classification problem, two Hermitian matrices (*i.e.*, observables)  $B_1$  and  $B_2$  were used in step 3 of both algorithms. Here, a matrix whose first five diagonal entries are one and whose other entries are zero was used as  $B_1$ . A matrix

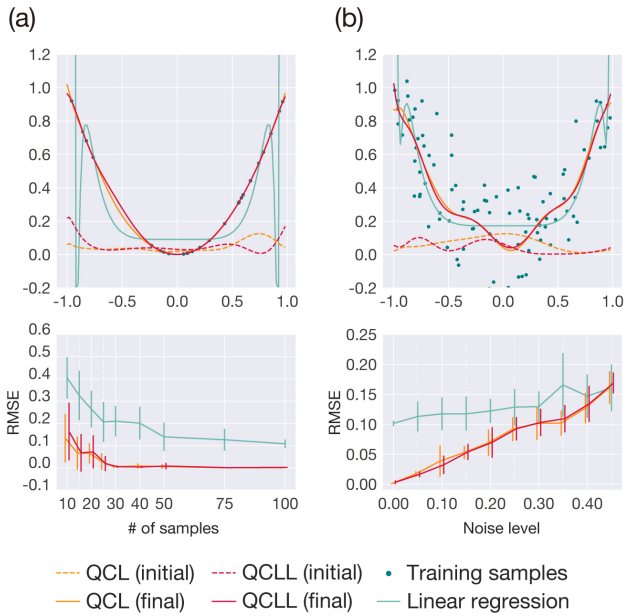


**FIG. 4.** Dependency of the models on the amount of training data and their robustness to noise. (a) Dependency on the amount of training data. QCL, QCLL, and a simple linear regression model were trained with a small number of samples ( $N = 25$ , top). The formats are the same as in Figure 2. The root mean squared error (RMSE) averaged across 10 simulation repetitions is plotted as a function of the number of training samples (bottom). (b) Robustness to noise. The three regression models were trained with training data including Gaussian noise ( $\sigma = 0.2$ , top). The formats are the same as in Figure 2. The RMSE averaged across 10 simulation repetitions is plotted as a function of the noise level (bottom).

whose 6–10-th diagonal entries are one and whose other entries are zero was used as  $B_2$ . The softmax function was used as the predefined function  $F(\cdot)$ . The cross-entropy function was used as the loss function  $E(\cdot, \cdot)$ . The number of qubits used to encode each input dimension was set to three, and the depth of the quantum circuit was set to three. The same optimization method as used in the previous regression task was used. The results are shown in Figure 3 (b) and 3(c). QCL and QCLL show similar behavior for this classification task.

Finally, using the same regression task, where  $f(x) = x^2$  was estimated, we investigated the dependency of the models on the amount of training data and their robustness to noise. In the analysis to investigate the dependency of the models on the amount of training data, the number of training samples was changed within the range from 10 to 100. In the analysis to investigate their robustness to noise, the models were trained with training data including Gaussian noise. The training data were generated in the same manner as in the previous regression analysis except that the target outputs  $y_n$  were set to  $f(\mathbf{x}_n) + \varepsilon_n$  where  $\varepsilon_n$  followed

a Gaussian distribution with a mean of zero and a standard deviation of  $\sigma$ .  $\sigma$  was varied within the range from 0.0 to 0.45. To quantitatively evaluate the prediction accuracy of a model trained with a given training data, we computed the root mean squared error (RMSE) between  $f(\mathbf{x})$  and the model prediction across points in  $[-1.0, 1.0]$ . As done in the Appendix of Mitarai et al. [26], as another machine-learning algorithm to be compared, we trained a simple linear regression model (*i.e.*, ordinary least squares) using  $\{x^6, x^5\sqrt{1-x^2}, x^4(1-x^2), x^3\sqrt{1-x^2}^3, x^2(1-x^2)^2, x\sqrt{1-x^2}^5, (1-x^2)^3\}$  as basis functions; these being polynomials appearing in  $|\psi_{\text{in}}(\mathbf{x})\rangle$  of QCL and  $\hat{\mathbf{v}}_{\text{in}}(\mathbf{x})$  of QCLL. As in Mitarai et al. [26], we examined how much QCL and QCLL avoided the risk of overfitting compared to this simple regression model.

To compare the dependency of the models on the amount of training data used, we evaluated the RMSE of each algorithm while changing the number of training samples (Figure 4(a)). In addition, to compare the robustness of the models to noise, we evaluated the RMSE of each algorithm while changing the level of Gaussian noise (Figure 4(b)). In both analyses, QCL and QCLL showed similar RMSEs, both of which were much lower than that of the simple linear regression. Those results suggest that QCL and QCLL efficiently avoid the risk of overfitting in similar manners.

#### IV. DISCUSSION AND CONCLUSIONS

We proposed a machine-learning algorithm with similar properties to quantum circuit learning (QCL). Our proposed algorithm, quantum circuit-like learning (QCLL) can be run on classical computers with  $O(Q)$  computational time and  $O(Q)$  required memory size, where  $Q$  is the hyperparameter corresponding to the number of qubits in QCL. The numerical simulations show that QCL and QCLL behave similarly on both regression and classification tasks (Figures 2 and 3). In addition, their similarities were consistently observed even when we changed the amount of training data and the level of noise (Figure 4). Therefore, our results suggest that, as a machine-learning algorithm, QCLL has similar properties, behavior and performance to QCL. This provides a new perspective with which to consider the computational and memory efficiency of quantum machine learning algorithms.

#### Acknowledgments

The authors would like to thank Shinji Nishimoto and Chikako Koide for preparing the environment for the analysis.

#### Funding

This research did not receive any specific grant from funding agencies in the public, commercial, or not-for-profit sectors.

#### Competing interests

All authors declare no competing financial interests.

## References

- [1] J. Preskill, *Quantum* **2**, 79 (2018).
- [2] A. Peruzzo, J. McClean, P. Shadbolt, M.-H. Yung, X.-Q. Zhou, P. J. Love, A. Aspuru-Guzik, and J. L. O’Brien, *Nature Communications* **5**, (2014).
- [3] J. R. McClean, K. J. Sung, I. D. Kivlichan, Y. Cao, C. Dai, E. S. Fried, C. Gidney, B. Gimby, P. Gokhale, T. Häner, T. Hardikar, V. Havlíček, O. Higgott, C. Huang, J. Izaac, Z. Jiang, X. Liu, S. McArdle, M. Neeley, T. O’Brien, B. O’Gorman, I. Ozfidan, M. D. Radin, J. Romero, N. Rubin, N. P. D. Sawaya, K. Setia, S. Sim, D. S. Steiger, M. Staudtner, Q. Sun, W. Sun, D. Wang, F. Zhang, and R. Babbush, ArXiv:1710.07629 [Physics, Physics:Quant-Ph] (2019).
- [4] B. Bauer, D. Wecker, A. J. Millis, M. B. Hastings, and M. Troyer, *Physical Review X* **6**, (2016).
- [5] A. Kandala, A. Mezzacapo, K. Temme, M. Takita, M. Brink, J. M. Chow, and J. M. Gambetta, *Nature* **549**, 242 (2017).
- [6] E. Farhi, J. Goldstone, and S. Gutmann, ArXiv:1411.4028 [Quant-Ph] (2014).
- [7] E. Farhi and A. W. Harrow, ArXiv:1602.07674 [Quant-Ph] (2019).
- [8] J. S. Otterbach, R. Manenti, N. Alidoust, A. Bestwick, M. Block, B. Bloom, S. Caldwell, N. Didier, E. S. Fried, S. Hong, P. Karalekas, C. B. Osborn, A. Pappageorge, E. C. Peterson, G. Prawiroatmodjo, N. Rubin, C. A. Ryan, D. Scarabelli, M. Scheer, E. A. Sete, P. Sivarajah, R. S. Smith, A. Staley, N. Tezak, W. J. Zeng, A. Hudson, B. R. Johnson, M. Reagor, M. P. da Silva, and C. Rigetti, ArXiv:1712.05771 [Quant-Ph] (2017).
- [9] M. Benedetti, E. Lloyd, S. Sack, and M. Fiorentini, *Quantum Science and Technology* **4**, 043001 (2019).
- [10] M. Benedetti, D. Garcia-Pintos, O. Perdomo, V. Leyton-Ortega, Y. Nam, and A. Perdomo-Ortiz, *Npj Quantum Information* **5**, (2019).
- [11] M. Benedetti, E. Grant, L. Wossnig, and S. Severini, *New Journal of Physics* **21**, 043023 (2019).
- [12] Y. Du, M.-H. Hsieh, T. Liu, and D. Tao, ArXiv:1810.11922 [Quant-Ph] (2018).
- [13] X. Gao, Z.-Y. Zhang, and L.-M. Duan, *Science Advances* **4**, eaat9004 (2018).
- [14] L. Cincio, Y. Subaşı, A. T. Sornborger, and P. J. Coles, *New Journal of Physics* **20**, 113022 (2018).
- [15] E. Farhi and H. Neven, ArXiv:1802.06002 [Quant-Ph] (2018).
- [16] M. Schuld and N. Killoran, *Physical Review Letters* **122**, (2019).
- [17] W. Huggins, P. Patil, B. Mitchell, K. B. Whaley, and E. M. Stoudenmire, *Quantum Science and Technology* **4**, 024001 (2019).
- [18] J.-G. Liu and L. Wang, *Physical Review A* **98**, (2018).
- [19] M. Schuld, A. Bocharov, K. Svore, and N. Wiebe, ArXiv:1804.00633 [Quant-Ph] (2018).
- [20] M. Fanizza, A. Mari, and V. Giovannetti, *IEEE Transactions on Information Theory* **65**, 5931 (2019).
- [21] M. Watabe, K. Shiba, M. Sogabe, K. Sakamoto, and T. Sogabe, ArXiv:1910.14266 [Physics, Physics:Quant-Ph] (2019).
- [22] P.-L. Dallaire-Demers and N. Killoran, *Physical Review A* **98**, (2018).
- [23] I. Cong, S. Choi, and M. D. Lukin, *Nature Physics* **15**, 1273 (2019).
- [24] K. Fujii and K. Nakajima, *Physical Review Applied* **8**, (2017).
- [25] S. Ghosh, A. Opala, M. Matuszewski, T. Patererek, and T. C. H. Liew, *Npj Quantum Information* **5**, (2019).
- [26] K. Mitarai, M. Negoro, M. Kitagawa, and K. Fujii, *Physical Review A* **98**, (2018).
- [27] S. Lloyd and C. Weedbrook, *Physical Review Letters* **121**, (2018).
- [28] J. Zeng, Y. Wu, J.-G. Liu, L. Wang, and J. Hu, *Physical Review A* **99**, (2019).
- [29] J. Romero and A. Aspuru-Guzik, ArXiv:1901.00848 [Quant-Ph] (2019).
- [30] M. Negoro, K. Mitarai, K. Fujii, K. Nakajima, and M. Kitagawa, ArXiv:1806.10910 [Quant-Ph] (2018).
- [31] T. Kusumoto, K. Mitarai, K. Fujii, M. Kitagawa, and M. Negoro, ArXiv:1911.12021 [Quant-Ph] (2019).
- [32] V. Havlíček, A. D. Córcoles, K. Temme, A. W. Harrow, A. Kandala, J. M. Chow, and J. M. Gambetta, *Nature* **567**, 209 (2019).
- [33] D. Zhu, N. M. Linke, M. Benedetti, K. A. Landsman, N. H. Nguyen, C. H. Alderete, A. Perdomo-Ortiz, N. Korda, A. Garfoot, C. Breche, L. Egan, O. Perdomo, and C. Monroe, *Science Advances* **5**, eaaw9918 (2019).
- [34] C. Zoufal, A. Lucchi, and S. Woerner, *Npj Quantum Information* **5**, (2019).
- [35] H. Situ, Z. He, Y. Wang, L. Li, and S. Zheng, ArXiv:1807.01235 [Quant-Ph] (2019).
- [36] L. Hu, S.-H. Wu, W. Cai, Y. Ma, X. Mu, Y. Xu, H. Wang, Y. Song, D.-L. Deng, C.-L. Zou, and L. Sun, *Sci Adv* **5**, eaav2761 (2019).
- [37] N. Pham and R. Pagh, in *Proceedings of the 19th ACM SIGKDD International Conference on Knowledge Discovery and Data Mining - KDD '13* (ACM Press, Chicago, Illinois, USA, 2013), p. 239.
- [38] R. Pagh, *ACM Transactions on Computation Theory* **5**, 1 (2013).
- [39] K. Weinberger, A. Dasgupta, J. Langford, A. Smola, and J. Attenberg, in *Proceedings of the 26th Annual International Conference on Machine Learning - ICML '09* (ACM Press, Montreal, Quebec, Canada, 2009), pp. 1–8.
- [40] M. Charikar, K. Chen, and M. Farach-Colton, *Theoretical Computer Science* **312**, 3 (2004).
- [41] K. M. Nakanishi, K. Fujii, and S. Todo, ArXiv:1903.12166 [Physics, Physics:Quant-Ph] (2019).
- [42] J. Li, X. Yang, X. Peng, and C.-P. Sun, *Physical Review Letters* **118**, (2017).
- [43] D. Kraft, *A Software Package for Sequential*

*Quadratic Programming* (Wiss. Berichtswesen d. DFVLR, 1988).